Eur Biophys J (2010) 39:213–227
DOI 10.1007/s00249-009-0521-2

ORIGINAL PAPER

Cholesterol modulation of nicotinic acetylcholine receptor surface mobility

Carlos J. Baier · Cristina E. Gallegos · Valeria Levi · Francisco J. Barrantes

Received: 25 May 2009 / Accepted: 6 July 2009 / Published online: 30 July 2009

Abstract Nicotinic acetylcholine receptor (AChR) function and distribution are quite sensitive to cholesterol (Chol) levels in the plasma membrane (reviewed by Barrantes in J Neurochem 103 (suppl 1):72–80, 2007). Here we combined confocal fluorescence recovery after photobleaching (FRAP) and confocal fluorescence correlation spectroscopy (FCS) to examine the mobility of the AChR and its dependence on Chol content at the cell surface of a mammalian cell line. Plasma membrane AChR exhibited limited mobility and only ~55% of the fluorescence was recovered within 10 min after photobleaching. Depletion of membrane Chol by methyl-β-cyclodextrin strongly affected the mobility of the AChR at the plasma membrane; the fraction of mobile AChR fell from 55 to 20% in Chol-depleted cells, whereas Chol enrichment by methyl-β-cyclodextrin-Chol treatment did not reduce receptor mobility at the cell surface. Actin depolymerization caused by latrunculin A partially restored receptor mobility in Chol-depleted cells. In agreement with the FRAP data, scanning FCS experiments showed that the diffusion coefficient of the AChR was about 30% lower upon Chol depletion. Taken together, these results suggest that membrane Chol modulates AChR mobility at the plasma membrane through a Chol-dependent mechanism sensitive to cortical actin.

Keywords Acetylcholine receptor · Lateral mobility · Lipid microdomains · Membrane · Nicotinic · Cholesterol

Abbreviations

αBTX	αBungarotoxin
AChR	Nicotinic acetylcholine receptor
BODIPY-FL-C5-SM	*N*-(4,4-difluoro-5, 7-dimethyl-4- bora-3a, 4a-diazo-s-indacene-3-pentanoyl)sphingosyl phosphocholine
CDx	Methyl-β-cyclodextrin
Chol	Cholesterol
CDx–Chol	Methyl-β-cyclodextrin–cholesterol
FCS	Fluorescence correlation spectroscopy
FRAP	Fluorescence recovery after photobleaching

Introduction

At the cholinergic synapse, the nicotinic acetylcholine receptor (AChR) converts the chemical signal of the neurotransmitter acetylcholine into a rapid electrical signal. The AChR is the prototype of the family of cys-loop receptors within the superfamily of rapid ligand-gated ion channels. In adult myotubes, this protein is highly concentrated in a small area juxtaposed to the nervous terminal, patched at the extraordinary density of 10,000–20,000 particles/μm^2, whereas in the rest of the plasma membrane its concentration is <10 particles/μm^2 (Barrantes 1979; Kummer et al. 2006).

Electronic supplementary material The online version of this article (doi:10.1007/s00249-009-0521-2) contains supplementary material, which is available to authorized users.

C. J. Baier · C. E. Gallegos · F. J. Barrantes (✉)
UNESCO Chair of Biophysics and Molecular Neurobiology, Instituto de Investigaciones Bioquímicas de Bahía Blanca, C.C. 857, B8000FWB Bahía Blanca, Argentina
e-mail: rtfjb1@criba.edu.ar

V. Levi
Laboratorio de Electrónica Cuántica, Departamento de Física, Universidad de Buenos Aires, 1428 Buenos Aires, Argentina

Several studies have demonstrated that the AChR is quite sensitive to the membrane lipid environment (reviewed in Barrantes 1993, 2004). Cholesterol (Chol) is an abundant component of the postsynaptic membrane (Barrantes 1989), and it has been demonstrated that this lipid affects the functional properties and distribution of the AChR (Barrantes 2003, 2004). Marsh and Barrantes (1978) demonstrated the lateral heterogeneity of lipids in the postsynaptic membranes of the Torpedo electrocyte: protein-associated lipids are immobilized with regard to bulk membrane lipid. Subsequent work has shown that Chol-like molecules form part of this protein-immobilized pool (Barrantes 2004; reviewed in 2007). The presence of Chol is important for maintaining agonist-dependent functional states of the AChR (Criado et al. 1982a). It has been proposed that there are two Chol populations in AChR-rich membranes from Torpedo: an easily extractable fraction that influences the bulk fluidity of the membrane and a tightly receptor-bound fraction (Leibel et al. 1987). Specific sites accessible to Chol have been identified in AChR transmembrane segments αM1, αM4, and γM4 (Corbin et al. 1998; Narayanaswami and McNamee 1993).

The lipid "raft" hypothesis proposes that specific lipid species self-associate to form microdomains or platforms that can intervene in protein partition (Simons and Ikonen 1997; Simons and van Meer 1988). There is some evidence that AChRs interact with Chol-rich lipid domains in vitro and in vivo (Bruses et al. 2001; Campagna and Fallon 2006; Marchand et al. 2002; Stetzkowski-Marden et al. 2006; Willmann et al. 2006; Zhu et al. 2006). In our laboratory it has been demonstrated that Chol plays a key role in the trafficking of the AChR along the secretory (Pediconi et al. 2004) and endocytic (Borroni et al. 2007) pathways and also affects AChR distribution in the plasma membrane (Borroni et al. 2007; Kellner et al. 2007).

The plasma membrane is a compartmentalized mosaic, the maintenance of which strongly depends on an active cytoskeleton network (Edidin 2003; Maxfield 2002). The pioneering study of Axelrod et al. (1976) using the fluorescence recovery after photobleaching (FRAP) technique demonstrated that in developing muscle cells the highly clustered AChRs present in large (20–60 μm) patches are practically immobile, with an effective lateral diffusion coefficient (D) of $<10^{-12}$ cm^2 s^{-1} (10^{-4} μm^2 s^{-1}), whereas more diffusely distributed AChRs in other regions of the same plasma membrane exhibit distinct, albeit slow, translational mobility ($D \sim 0.5 \times 10^{-2}$ μm^2 s^{-1}). Receptor mobility displays a strong dependence on cytoskeletal integrity (Bloch et al. 1989; Dai et al. 2000; Pumplin 1989).

In this work, the 2D mobility of the AChR at the plasma membrane and its dependence on membrane Chol levels were first studied using the FRAP technique in the confocal mode (Ellenberg et al. 1997; Nehls et al. 2000; Zaal et al. 1999). Briefly, in this ensemble method a defined 2D region was selected from the confocal section of the cell membrane, thus restricting the analysis to a few thousand fluorescence-tagged AChRs. The region was photobleached by transiently increasing the laser power of the confocal microscope, and the diffusive exchange of bleached proteins with nearby unbleached molecules was then followed using low-intensity laser excitation. Recovery into the bleached region can be described by two properties, an apparent lateral diffusion coefficient, D, and a mobile fraction, Mf (reviewed by Chen et al. 2006, Edidin 1994, and Guo et al. 2008). D provides a measure of the kinetics of translational mobility whereas Mf is indicative of the fraction of fluorescent molecules that are able to recover in the bleached area over the time course of the assay (Kenworthy et al. 2004). FRAP has been used extensively to characterize protein and lipid diffusional mobility and the domain structure of the plasma membrane, typically by monitoring recoveries in small spots (approx. 1 μm^2; Edidin 1994). Here, as in Kenworthy et al. (2004), bleaching and monitoring of recovery kinetics were followed into an area of the membrane much larger than the proposed size of lipid microdomains (Jacobson et al. 2007; Rao and Mayor 2005). Diffusional recovery would require either the diffusion of entire domains or the diffusion of individual proteins outside such domains.

CHO-K1/A5 is a clonal cell line developed in our laboratory that stably expresses heterologous adult murine muscle-type AChR (Roccamo et al. 1999). We have recently shown that in these cells the AChR aggregates in the form of very small, nanometer-sized clusters (Kellner et al. 2007), although the cells lack rapsyn and other receptor-anchoring proteins. This allows one to study the inherent mobility/dynamics of AChR assemblies in the absence of receptor-anchoring molecules and provides a convenient minimalist approach to defining the crosstalk between the AChR protein and the neutral lipid, cholesterol. Here we study the dynamics of the AChR at the plasma membrane of CHO-K1/A5 cells and show that the lateral mobility of the AChR is affected by Chol depletion, this effect being reversed when cells are treated with methyl-β-cyclodextrin–Chol (CDx–Chol) complexes. We also show the involvement of the cytoskeleton network in the Chol-dependent dynamics of the receptor at the plasmalemma.

Materials and methods

Materials

Alexa-labeled α-bungarotoxins (alexa^{488}-αBTX and alexa^{647}-αBTX), alexa^{488}-labeled anti-rat antibody, and the fluorescent sphingomyelin (SM) probe *N*-(4,4-difluoro-

5,7-dimethyl-4-bora-3a,4a-diazo-s-indacene-3-pentanoyl) sphingosyl-phosphocholine (BODIPY-FL-C_5-SM) were purchased from Molecular Probes (Eugene, OR, USA). Latrunculin A, methyl-β-cyclodextrin (CDx), and mAb210 anti-AChR monoclonal antibody were obtained from Sigma (St Louis, MO, USA). The ester of poly(ethylene glycol)-derivatized cholesterol (fPEG-Chol) was kindly provided by Professor Toshihide Kobayashi and Dr Satoshi B. Sato of the Lipid Biology Laboratory, RIKEN Institute of Physical and Chemical Research, Discovery Research Institute, Saitama, Japan, and Department of Biophysics, Kyoto University, Japan, respectively.

Cell culture

Before fluorescence microscopy experiments, CHO-K1/A5 cells were grown in Ham's F12 medium supplemented with 10% bovine fetal serum (BFS) for 2–3 days at 37°C as in Roccamo et al. (1999).

cDNA transfections

Plasmids for rapsyn-GFP (green fluorescent protein-labeled rapsyn) were kindly provided by Dr Jonathan Cohen, Harvard University. CHO-K1/A5 cells were grown in Ham's F-12 medium supplemented with 10% BFS for 24 h and then transfected with 1.5 μg DNA/35-mm dish of rapsyn-GFP using the PolyFect transfection Reagent (Qiagen) for 24 h according to the manufacturer's recommendations.

Acute Chol depletion/enrichment of cultured cells

Acute Chol depletion prior to fluorescence labeling was accomplished by treating CHO-K1/A5 cells with 10–15 mM CDx in medium 1 ("M1": 140 mM NaCl, 1 mM $CaCl_2$, 1 mM $MgCl_2$, and 5 mM KCl in 20 mM HEPES buffer, pH 7.4) essentially as in Borroni et al. (2007) except that incubation proceeded for 20 min at 37°C. In order to increase the Chol content of the cells, CDx–Chol complexes were prepared as in Christian et al. (1997) and CHO-K1/A5 cells were incubated with 3.5–10 mM Chol–CDx complexes (CDx:Chol 6:1) at 37°C for 20 min. For chronic Chol depletion, CHO-K1/A5 cells were treated with 1 μM mevinolin for 24 h in nutridoma medium containing 0.1% BFS, as in Pediconi et al. (2004).

Disruption of the cortical actin meshwork with latrunculin A

In order to disrupt the cortical cytoskeletal meshwork, CHO-K1/A5 cells were incubated with 20 μM latrunculin A together with 10–15 mM CDx (control cells only with the CDx vehicle, M1).

Labeling of cells with fluorescent probes

To label CHO-K1/A5 cells with the fluorescent Chol analog they were treated with 10-15 mM CDx as described above and then labeled with fPEG-Chol (0.25–1 μM) for 5–10 min at room temperature, washed with M1, and mounted for microscopy. Similarly, labeling with the fluorescent SM analog BODIPY-FL-C_5-SM at a final concentration of 0.3 μM was carried out on control and Chol-depleted CHO-K1/A5 cells for 10 min at room temperature. In order to label plasma membrane AChR, CHO-K1/A5 cells were stained with alexa^{488}-αBTX or alexa^{647}-αBTX at a final concentration of 1 μM for 1 h at 4°C in M1, washed, and mounted for microscopy.

Crosslinking of plasma membrane AChR in CHO-K1/A5 cells was accomplished by labeling of cells with mAb210 monoclonal antibody for 1 h at 4°C in M1, washing, and labeling with alexa^{488}-labeled anti-rat antibody for 1 h at 4°C in M1, followed by washing and final mounting for microscopy.

Live cell confocal fluorescence recovery after photobleaching imaging

Fluorescence recovery after photobleaching (FRAP) experiments were carried out using a Leica TCS SP2 microscope (Leica Microsystems, Heidelberg, Germany). The fluorescent probes were excited according to their excitation spectra: fPEG-cholesterol, BODIPY-FL-C_5-SM, and alexa^{488}-αBTX using the 488 nm line of an argon laser, alexa^{647}-αBTX using the 633 nm line. A 63× 1.4 NA water-immersion objective was used for imaging with the pinhole diameter set for 1 Airy unit. Time and laser power for the photobleaching step (100%) were determined for each fluorescent probe. The region of interest (ROI) used in the analysis was $\sim 6\ \mu m^2$. Pre and post-bleach images were obtained at low laser power in order to minimize photodamage of fluorescent dyes. The average fluorescent intensity within the bleach ROI was normalized to the pre-bleach intensity for each time point. Fluorescence recovery kinetics were determined by exponential fitting of the averaged data using Eq. 1:

$$f(x) = \sum_{i=1}^{n} A_i(1 - e^{(-t/\tau i)}) \quad (1)$$

where A_i is the amplitude of each component, t is time, and τ_i is the time constant of each component. The mobile fraction (Mf) was calculated using Eq. 2:

$$\mathrm{Mf} = \frac{(F_\infty - F_0)}{(F_\mathrm{i} - F_0)} \quad (2)$$

where F_∞ is the fluorescence intensity at the end of the FRAP experiment, F_i is the initial fluorescence intensity

prior to the photobleaching steps, and F_0 is the fluorescence intensity immediately after photobleaching. The diffusion coefficient was calculated as in Ellenberg et al. (1997). Analysis of FRAP data was carried out using Leica Confocal LCS Lite version 2.61 (Leica Microsystems) and the Origin laboratory package (OriginLab, MA, USA).

Confocal fluorescence correlation spectroscopy microscopy

Fluorescence correlation spectroscopy (FCS) experiments were carried out using an Olympus Fluoview 1000 confocal microscope. The excitation source was a multi-line Ar laser tuned at 488 nm (average power at the sample, 700 nW). The laser light was reflected by a dichroic mirror (DM405/488) and focused through an Olympus UPlanSApo 60× oil immersion objective (NA = 1.35) on to the sample. The fluorescence was collected by the same objective, passed through a 105 μm pinhole, reflected on a diffraction grating, and passed through a slit set to transmit in the range 500–600 nm. Fluorescence was detected by a photomultiplier set in photon-counting detection mode.

Transmission images of the cells were collected simultaneously with confocal imaging by using an external photomultiplier detector that collects the light of the excitation laser transmitted through the sample. We compared these images with the corresponding confocal images to facilitate detection of the plasma membrane area under study in the living cells. Linear scanning confocal-FCS experiments were done by scanning at a speed of 40 μs/pixel. The frequency of the line scanning was varied between 150 and 200 Hz.

Line-FCS data were analyzed using Globals for Images, a program developed by E. Gratton at the Laboratory for Fluorescence Dynamics (UCI, Irvine, CA, USA). Scanning-FCS experiments were analyzed in a manner similar to that described by Ruan et al. (2004) with some modifications. Briefly, the normalized autocorrelation function was calculated for every pixel of the line as:

$$G_i(\tau) = \frac{\langle I_i(t) \times I_i(t+\tau)\rangle - \langle I_i(t)\rangle^2}{\langle I_i(t)\rangle^2} \quad (3)$$

where $I_i(t)$ is the fluorescence intensity recorded at the pixel i and τ is a lag time. This function characterizes the time-dependent decay of the fluorescence fluctuations to their equilibrium value and thus provides information regarding the process that produces the fluctuation.

We fitted the experimental autocorrelation data with Eq. 4, which is obtained considering free diffusion of the receptor and a 3D Gaussian beam profile (recently reviewed by Muller et al. 2003):

$$G(\tau) = G_o \frac{1}{\left(1+\frac{4D\tau}{\varpi_o^2}\right)\sqrt{\left(1+\frac{4D\tau}{z_o^2}\right)}} \quad (4)$$

where D is the diffusion coefficient of the molecule and ω_o and z_o are the radial and axial waists of the point spread function, respectively. These latter parameters were calibrated in an independent experiment by measuring the autocorrelation function of a sample with known diffusion coefficient. This calibration was done by measuring the autocorrelation curve of the fluorescent probe fluorescein at pH 8 ($D_{\text{fluorescein}} = 300\ \mu m^2\ s^{-1}$; Ruan et al. 2004). G_o is related to the average number of molecules in the observation volume (N) according to:

$$G_o = \frac{\gamma}{N} \quad (5)$$

where γ is a geometric parameter equal to 0.35 for a Gaussian beam profile. The data are presented as average ± standard error, which are calculated from the standard deviation obtained from different line measurements.

Results

Dynamics of fluorescent lipid probes at the plasma membrane of CHO-K1/A5 cells

We initially set out to study whether Chol depletion from the plasma membrane affected the mobility of two different fluorescent lipid probes. fPEG-Chol was tested first. This fluorescent probe labels Chol-rich zones exclusively in the outer plasma membrane of live cells (Ishitsuka et al. 2005; Sato et al. 2004). In order to verify the efficacy of the Chol depletion procedure, CHO-K1/A5 cells were treated with 10 mM CDx and then labeled with fPEG-Chol (0.25–1 μM) for 5–10 min at room temperature. The fluorescence intensity of plasma membrane fPEG-Chol (Fig. 1a) provided a direct in situ assessment of Chol levels at the cell surface, thus complementing chemical assays of Chol levels in whole cells and isolated membranes (Borroni et al. 2007). fPEG-Chol fluorescence decreased by up to 70% in Chol-depleted cells compared with control cells (i.e. incubated with the drug vehicle only), in agreement with the results of Sato et al. (2004) and our own chemical determinations in whole CHO-K1/A5 cells (Borroni et al. 2007), indicating that CDx treatment effectively depleted the cell-surface Chol pool.

In the FRAP experiments, a small region of the plasma membrane labeled with fPEG-Chol was bleached using the 488 nm laser line and the fluorescence recovery was monitored as a function of time (Fig. 1b, c). As described in "Materials and methods", the fluorescence recovery within the bleached region was normalized to the pre-bleach

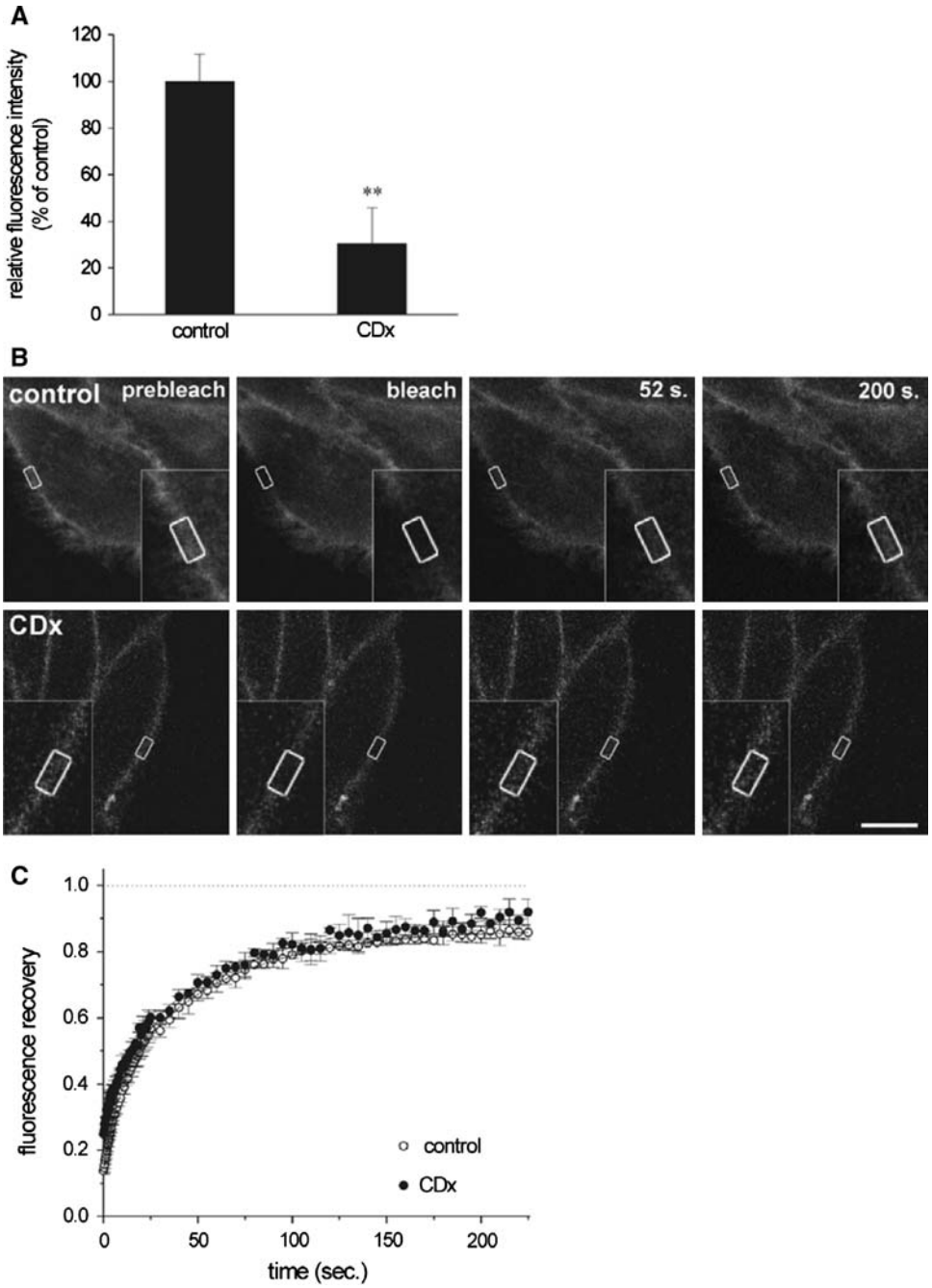

Fig. 1 Confocal fluorescence recovery after photobleaching (FRAP) of the Chol analog fPEG-Chol at the plasma membrane of CHO-K1/A5 cells. **a** Relative fluorescence intensity of the fPEG-Chol in control and Chol-depleted (CDx-treated) cells. **b** FRAP time series of fPEG-Chol-labeled cells. The ROI delimited by the *white box* was bleached and the fluorescence recovery was followed for a total of 4 min. The *insets* show higher magnifications of the bleached region. **c** Averaged FRAP curves. Fluorescence at each point after photobleaching (bleach time, $t = 0$) was normalized to pre-bleaching intensity. *Dotted line* two-exponential fit to experimental data (average of three independent experiments, 10–15 cells analyzed in each case). The *double asterisk* denotes a statistically significant difference, $P < 0.01$. *Bar* 10 μm

intensity and the resulting data were fitted to Eq. 1. The ratio of observed recovery to the initial fluorescence yielded an estimate of the mobile fraction (Mf) of labeled molecules (Eq. 2). Following the photobleach, fPEG-Chol showed an Mf of ~85% (Fig. 1c; Table 1) during the 4 min of the recovery period, and no differences were observed in this parameter between control and Chol-depleted cells (see Table 1). As shown in Supplementary Fig. 1, the fluorescence recovery kinetics of fPEG-Chol fitted better with a two-exponential than with a single-exponential function (Fig. 1c).

Table 1 Mobile fraction (Mf) and diffusion coefficient (D) values of fluorescent lipid probes and αBTX-labeled AChR under control or Chol-depletion conditions

Condition	Mf	D ($\mu m^2\ s^{-1}$)
fPEG-cholesterol		
Control cells	0.83 ± 0.02	$8.3 \pm 1.3 \times 10^{-2}$
10 mM CDx	0.86 ± 0.03	$5.9 \pm 0.6 \times 10^{-2}$*
BODIPY FL C_5-SM		
Control cells	0.82 ± 0.09	$5.2 \pm 0.4 \times 10^{-2}$
10 mM CDx	0.82 ± 0.02	$4.2 \pm 1.1 \times 10^{-2}$
αBTX-labeled AChR		
Control cells	0.56 ± 0.09	$0.46 \pm 0.09 \times 10^{-2}$
10 mM CDx	0.19 ± 0.12*	$0.27 \pm 0.08 \times 10^{-2}$*
Control + 20 μM latrunculin A	0.44 ± 0.04	$0.67 \pm 0.18 \times 10^{-2}$
10 mM CDx + 20 μM latrunculin A	0.28 ± 0.10	$0.49 \pm 0.21 \times 10^{-2}$
3.5 mM CDx–Chol (6:1)	0.62 ± 0.08	$0.63 \pm 0.26 \times 10^{-2}$
10 mM CDx–Chol (6:1)	0.54 ± 0.10	$1.17 \pm 0.44 \times 10^{-2}$*

The averaged data correspond to three independent experiments (10–15 cells analyzed in each case). Mf was calculated using Eq. 2 and D values were obtained as in Ellenberg et al. (1997). Asterisks denote statistically significant differences, $P < 0.05$

The second fluorescence lipid probe tested, a derivative of SM (BODIPY-FL-C_5-SM), is reported to be a fluid phase marker (Hao et al. 2001). Control and Chol-depleted cells (10 mM CDx) were labeled with 0.3 μM BODIPY-FL-C_5-SM for 10 min at room temperature (Fig. 2a). A small (~25%) but statistically significant increase in fluorescence intensity of plasma membrane BODIPY-FL-C_5-SM was apparent in Chol-depleted cells compared with untreated cells (Fig. 2a, b). This result is in agreement with the diminution in generalized polarization of the fluorescent probe laurdan in CHO-K1/A5 plasma membranes treated with CDx (Borroni et al. 2007): the behavior of both probes indicates that the membrane becomes more "fluid" upon Chol depletion. As was the case with fPEG-Chol, the fluorescence recovery kinetics of BODIPY-FL-C_5-SM fitted better with a two-exponential rather than a single-exponential function (data not shown). BODIPY-FL-C_5-SM showed an Mf of ~80% (Fig. 2c; Table 1) during the 4-min recovery period following the photobleach, and no differences were observed between the Mf values of control and Chol-depleted cells (c.f. Table 1).

The lateral mobility of AChR at the plasma membrane of CHO-K1/A5 cells is affected by changes in Chol content

In the next series of FRAP experiments we studied the lateral mobility of AChR at the plasma membrane of CHO-K1/A5 cells labeled with alexa^{488}-αBTX, a fluorescent quasi-irreversible antagonist which stably labels plasma membrane receptors (Borroni et al. 2007), and investigated whether receptor mobility was affected by Chol content. In control cells, the fluorescence recovery kinetics could be fitted using either one or two-exponential curves, the single-exponential fit yielding a statistically more significant result (Supplementary Fig. 1). As expected, the fluorescence recovery of the AChR (Fig. 3) was one order of magnitude slower than that observed for the fluorescent lipid probes (Figs. 1, 2). The t_{50} for fPEG-Chol, BODIPY-FL-C_5-SM, and fluorescent αBTX-AChR conjugates were about 20, 30, and 210 s, respectively. Following the photobleach, fluorescent αBTX-AChR conjugates showed a mobile fraction (Eq. 2) of roughly 50% during the 10 min recovery period (Fig. 3; Table 1).

When the plasma membrane of CHO-K1/A5 cells is depleted of Chol, the amount of AChR at the cell surface decreases by about 50% (Fig. 3a) as a result of the dramatically enhanced endocytosis triggered by Chol depletion (Borroni et al. 2007). Concomitantly, the fluorescence recovery of the toxin-labeled receptor was clearly slower than in control cells (Fig. 3b, c). The decrease in the AChR mobile fraction (from ~50% in control cells to only ~20% in CDx-treated cells) was statistically significant (Fig. 3c; Table 1). Chronic Chol depletion of CHO-K1/A5 cells by the drug mevinolin (Pediconi et al. 2004) produced similar effects on AChR mobility at the plasma membrane (see Supplementary Fig. 2).

Next we analyzed the behavior of the AChR upon treatment with CDx–Chol complexes, prepared as in Christian et al. (1997). These authors demonstrated that by using different CDx:Chol proportions it is possible to modify the cellular Chol content. In previous work we determined that Chol depletion caused gain-of-function, whereas Chol enrichment had the opposite effect on single-channel mean open time distribution as assayed by single-channel patch-clamp recordings (Borroni et al. 2007). We used a CDx:Chol ratio of 6:1, as in Borroni et al. (2007). Cells were incubated with CDx–Chol at concentrations of 3.5–10 mM (Fig. 4). As shown in Fig. 4, no statistically significant differences were observed between control cells and cells treated with CDx–Chol complexes, in contrast with the behavior of cells incubated with CDx alone (Fig. 3). FRAP recovery kinetics of the AChR labeled with fluorescent αBTX in CHO-K1/A5 cells incubated with CDx–Chol complexes (Fig. 4b) differed noticeably from those of Chol-depleted cells (compare the curves in Figs. 3c and 4b). No statistically significant differences were apparent between control and CDx–Chol treated cells in the percentage of the mobile fraction (c.f. Table 1).

We analyzed the mobility of AChR in CHO-K1/A5 cells transiently expressing rapsyn-GFP. As shown in

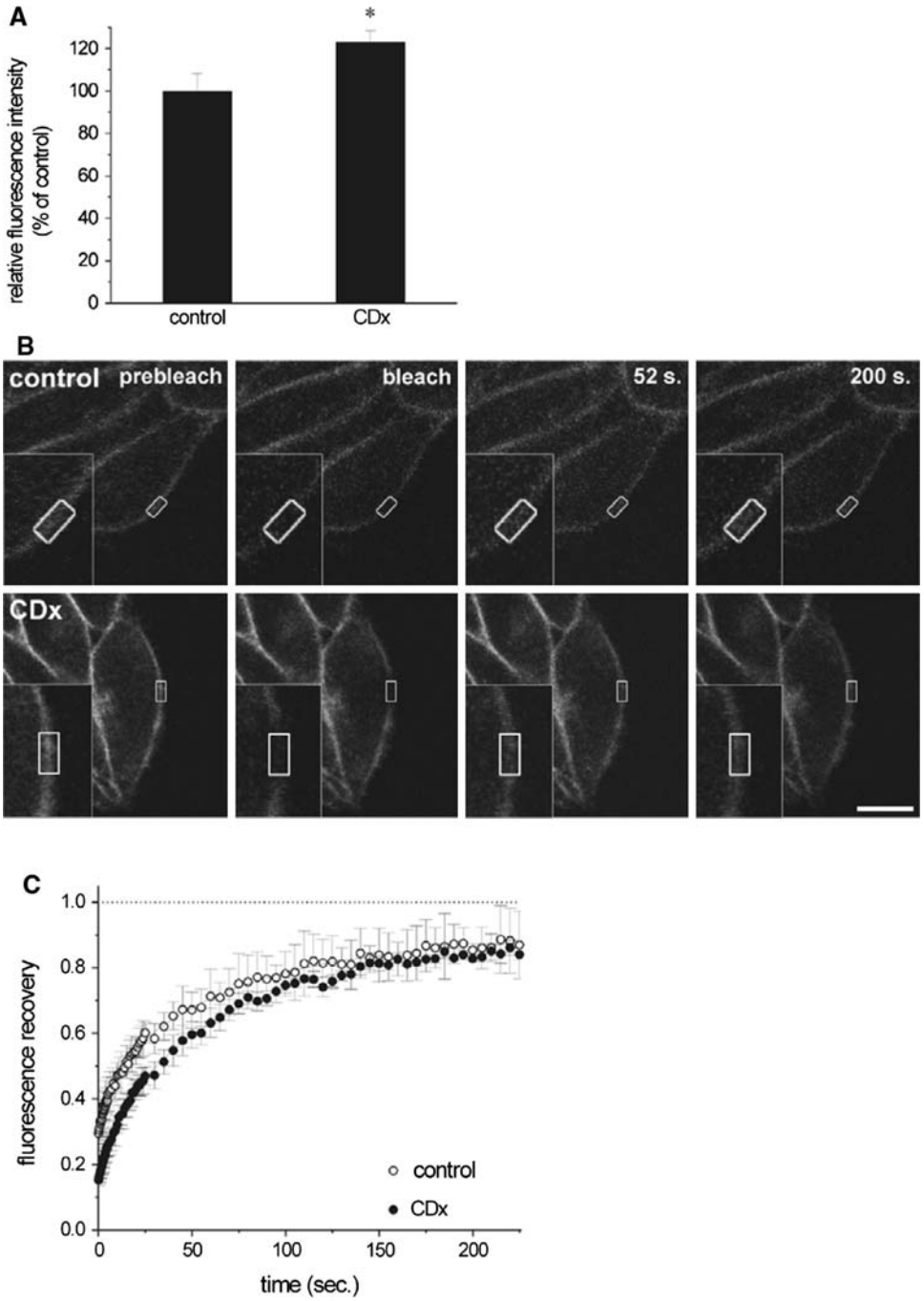

Fig. 2 FRAP of the SM fluorescent probe BODIPY-FL-C_5-SM at the plasma membrane of CHO-K1/A5 cells. **a** Fluorescence intensity of control and Chol-depleted (CDx-treated) CHO-K1/A5 cells. **b** FRAP series in control and CDx-treated cells. The region delimited by the *white box* was bleached and the fluorescence recovery followed for 4 min. The *insets* show enlargements of the bleached region. **c** Averaged FRAP curves. Fluorescence at each point after photobleaching (bleach time, $t = 0$) was normalized to pre-bleaching intensity. Two-exponential fits to experimental data are shown as *dotted lines*. The averaged data correspond to three independent experiments (10–15 cells each). The *asterisk* denotes a statistically significant difference, $P < 0.05$. *Bar* 10 μm

Supplementary Fig. 3A, cells that co-express AChR and rapsyn-GFP showed a diffuse distribution of both proteins at the plasma membrane. Crosslinking of AChR in living cells via extracellular ligands changed the distribution of intracellular rapsyn-GFP, from a diffuse to a patched distribution; furthermore, rapsyn clusters colocalized with AChR patches (Supplementary Fig. 3B), indicating that in CHO-K1/A5 cells the AChR and rapsyn-GFP interact at the plasma membrane. When AChR mobility was analyzed by the FRAP technique in rapsyn-GFP-expressing cells,

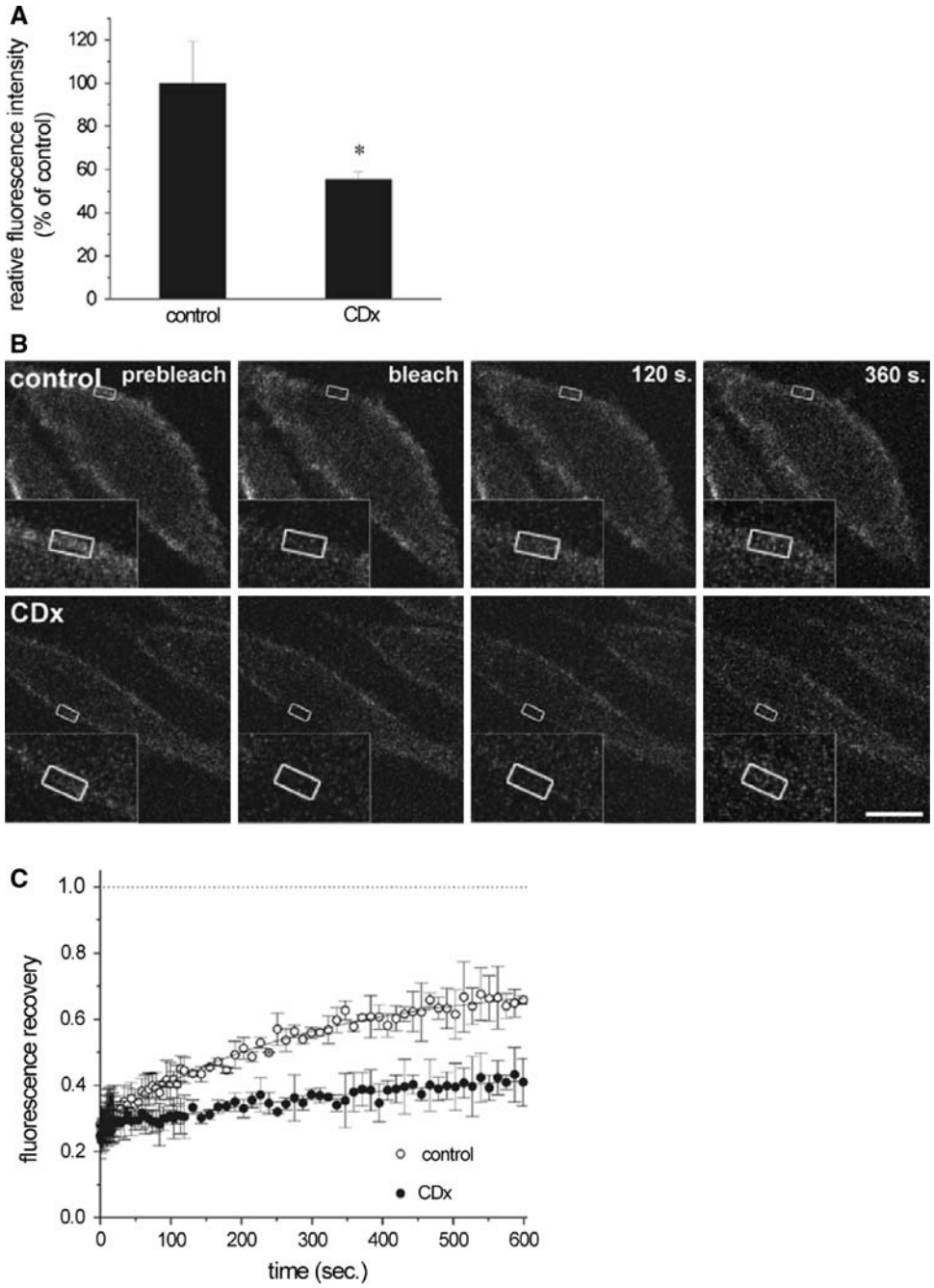

Fig. 3 FRAP of plasma membrane AChR is affected by Chol depletion. **a** Plasma membrane fluorescence intensity of CHO-K1/A5 cells labeled with fluorescent αBTX, in control and CDx-treated cells. **b** Images from a FRAP series in control and CDx-treated cells. The region delimited by the *white box* was bleached and the fluorescence recovery followed for 10 min. The *insets* show enlargement of the bleached region. **c** Averaged FRAP curves for control and CDx-treated cells. Fluorescence at each point after photobleaching (bleach time, $t = 0$) was normalized to pre-bleaching intensity. Single-exponential curves fitting the experimental data points are shown as *dotted lines*. The averaged data correspond to three independent experiments (10–15 cells analyzed in each case). The *asterisk* denotes a statistically significant difference, $P < 0.05$. *Bar* 10 μm

AChR diffusion at the plasma membrane was found to be slower than that in cells that do not express rapsyn (Supplementary Fig. 3C, compare with main Fig. 3c). These results could reflect the association between AChR and rapsyn-GFP in our system and show that association of AChR with non-receptor proteins located at the cytosolic surface of the plasma membrane slows down its lateral mobility.

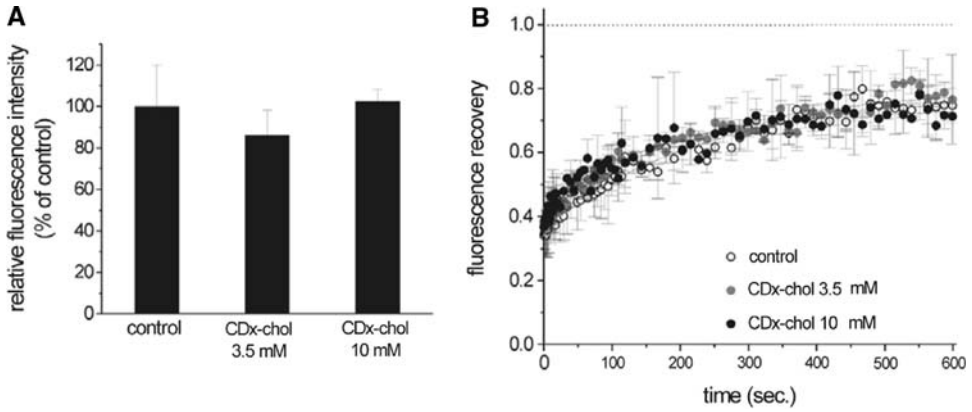

Fig. 4 Chol enrichment of CHO-K1/A5 cells with CDx–Chol complex did not reduce AChR mobility. **a** Plasma membrane fluorescence intensity of CHO-K1/A5 cells labeled with fluorescent αBTX, in control and 3.5–10 mM CDx–Chol-treated cells. **b** Averaged FRAP curves for control and CDx-treated cells. Fluorescence at each point after photobleaching (bleach time, $t = 0$) was normalized to pre-bleaching intensity. Single-exponential curves fitting the experimental data points are shown as *dotted lines*. The averaged data correspond to three independent experiments (10–15 cells analyzed in each case)

The alteration in plasma membrane AChR mobility by Chol depletion involves cytoskeletal integrity

Several reports have described the relationship between the Chol content of biological membranes and the cytoskeleton (reviewed by Maxfield 2002). We recently observed that Chol depletion from the plasma membrane of CHO-K1/A5 cells results in an increase in the size of antibody-induced AChR nano-clusters and changes in the long-range organization of the AChR (Kellner et al. 2007). We surmised that the cytoskeleton could be involved in this phenomenon. In order to experimentally test this hypothesis, cells were treated with 20 μM latrunculin A, an agent that strongly inhibits actin polymerization (Coue et al. 1987; Spector et al. 1989), together with 10 mM CDx (control cells were treated only with latrunculin A and the vehicle of CDx, M1). In the presence of latrunculin A, the amount of AChR at the plasma membrane decreased upon Chol depletion (Fig. 5a), but no statistical differences were observed between the fluorescence recovery kinetics of fluorescent αBTX-labeled AChR in control and Chol-depleted cells (Fig. 5b). Similarly, the mobile fraction of control and latrunculin/CDx-treated cells showed no statistically significant differences (Table 1). These results suggest that blockage of actin cytoskeletal dynamics by latrunculin A partially inhibits the CDx-mediated effects of Chol depletion on receptor lateral mobility.

AChR diffusion coefficient is sensitive to plasma membrane Chol content

The diffusion coefficient, D, of the AChR at the plasma membrane of CHO-K1/A5 cells, calculated as in Ellenberg et al. (1997), is shown in Table 1. AChR mobility was severely affected when plasma membrane Chol was substantially reduced by CDx treatment: the diffusion coefficient fell by about 40% upon Chol depletion (0.27×10^{-2} μm^2 s^{-1}), as was clearly apparent from the fluorescence recovery curves (Fig. 3c). These differences in AChR diffusion coefficient between control and Chol-depleted cells disappeared when cells were incubated with CDx in the presence of latrunculin A (Table 1), suggesting that in CHO-K1/A5 cells, as in other AChR-constitutive expression models, the receptor is associated to the cytoskeleton (Bloch et al. 1989; Dai et al. 2000; Pumplin 1989). This result reinforces the suggestion that the alteration of the topological relationship between AChR clusters upon Chol depletion could result, at least in part, from disruption of AChR–cytoskeleton interactions (Kellner et al. 2007). In Chol-enriched CHO-K1/A5 cells (i.e. cells treated with CDx–Chol complexes) the diffusion coefficient of the AChR macromolecule increased, as reported for the EGFR (Orr et al. 2005).

Antibody-mediated AChR crosslinking abolishes receptor mobility

In recent work, Sieber et al. (2007) determined that plasma membrane clusters of syntaxin depend on weak homophilic protein–protein interactions, and that syntaxin molecules in these clusters are dynamically exchanged with freely diffusing molecules. AChRs at the plasma membrane of CHO-K1/A5 cells are present in the form of nano-clusters with an average diameter of about 55 nm (Kellner et al. 2007). Cell-surface AChRs in CHO-K1/A5 cells were crosslinked with mAb210 monoclonal anti-AChR antibodies followed by staining with alexa^{488}-labeled secondary antibodies, and AChR dynamics were investigated with FRAP on these live specimens. As shown in Fig. 6, no fluorescence recovery was observed during the course of the FRAP experiment

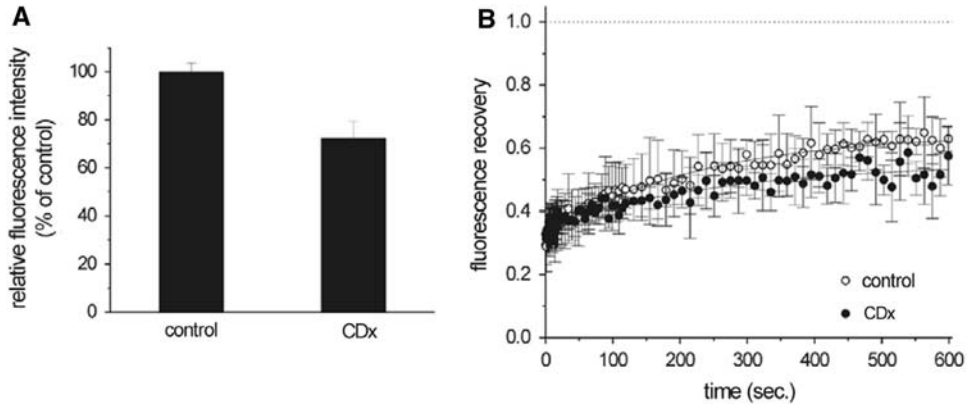

Fig. 5 Coincubation of latrunculin A with CDx partially abolishes the changes in FRAP in Chol-depleted cells. **a** CHO-K1/A5 cells were coincubated with 20 μM latrunculin A together with 10 mM CDx or M1, respectively, and plasma membrane fluorescence intensity of αBTX-labeled cells was measured. **b** Averaged FRAP curves for control and CDx-treated cells. Fluorescence at each point after photobleaching (bleach time, $t = 0$) was normalized to pre-bleaching intensity. Single-exponential curves fitting the experimental data points are shown as *dotted lines*. The averaged data correspond to three independent experiments (10–15 cells analyzed in each case)

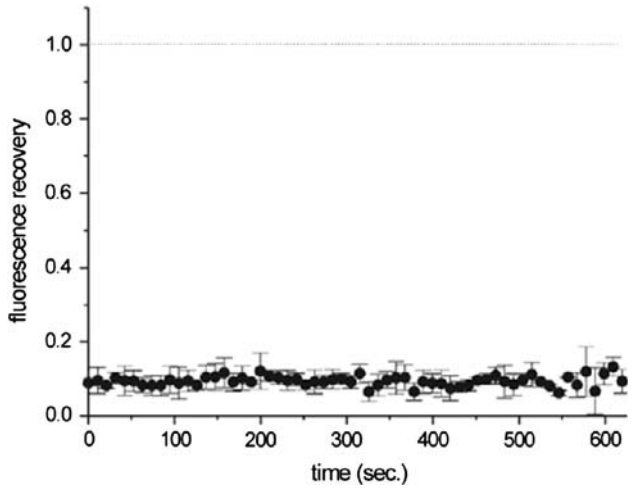

Fig. 6 Abolition of AChR mobility by antibody crosslinking. Average FRAP trace for AChR labeled with primary (mAb210) and secondary fluorescent antibody. No recovery was observed over a period of 10 min. Fluorescence at each point after photobleaching (bleach time, $t = 0$) was normalized to pre-bleaching intensity. The averaged data correspond to three independent experiments

(10 min) or up to periods of 20 min (data not shown) under these conditions. The lack of fluorescence recovery suggests that crosslinking recruits and immobilizes the mobile fraction of AChRs observed with fluorescent αBTX labeling, i.e. in the absence of antibody-induced crosslinking, in agreement with AChR crosslinking studies in rat myotubes in primary culture (Axelrod 1980).

Cholesterol-dependent mobility of AChR in small membrane areas revealed by confocal-FCS experiments

We next studied the effect of CDx on the mobility of AChR receptor by using scanning-FCS in the confocal microscope. CHO-K1/A5 cells were labeled with alexa^{488}-αBTX and incubated in the absence or presence of CDx as described in previous sections. In these experiments the laser traces a line across the cell membrane in a repetitive fashion, and the intensity at each pixel of the line is recorded as a function of time. Figure 7 shows an example of scanning-FCS data taken for a control CHO-K1/A5 cell. The data are represented as a matrix in which the intensity measured along the line is plotted as a function of the line number. In this particular example, the intensity at the positions included in the dotted red box is higher, showing that in this region the laser crossed the membrane. We calculated the autocorrelation function at each pixel of the line and observed that whereas there is no correlation in the cell cytoplasm or the extracellular milieu, there is a clear autocorrelation at positions where the line scanning hits the membrane (Fig. 7c). Because the line-acquisition frequency is very low, fluctuations due to fast-moving molecules (e.g. free alexa^{488}-αBTX, if any) are averaged out and thus are not detected in these experiments.

The autocorrelation function was calculated for every pixel at membrane positions using Eq. 4. Table 2 shows the average values of G_o and D obtained from 60 different line scans in 20 control and 20 CDx-treated CHO-K1/A5 cells. The diffusion coefficient of AChR in CDx-treated cells was about 30% lower than in control cells, showing that Chol depletion slows down the motion of the AChR ($P < 0.001$), a conclusion in agreement with the FRAP experiments. Furthermore, G_o values were $\sim$20% higher in CDx-treated cells. G_o is inversely related to the number of molecules in the observation volume; thus, the average number of receptor molecules is lower in CDx-treated cells than in control cells (Student's t test, $P < 0.005$). The result of this dynamic measurement is in full agreement

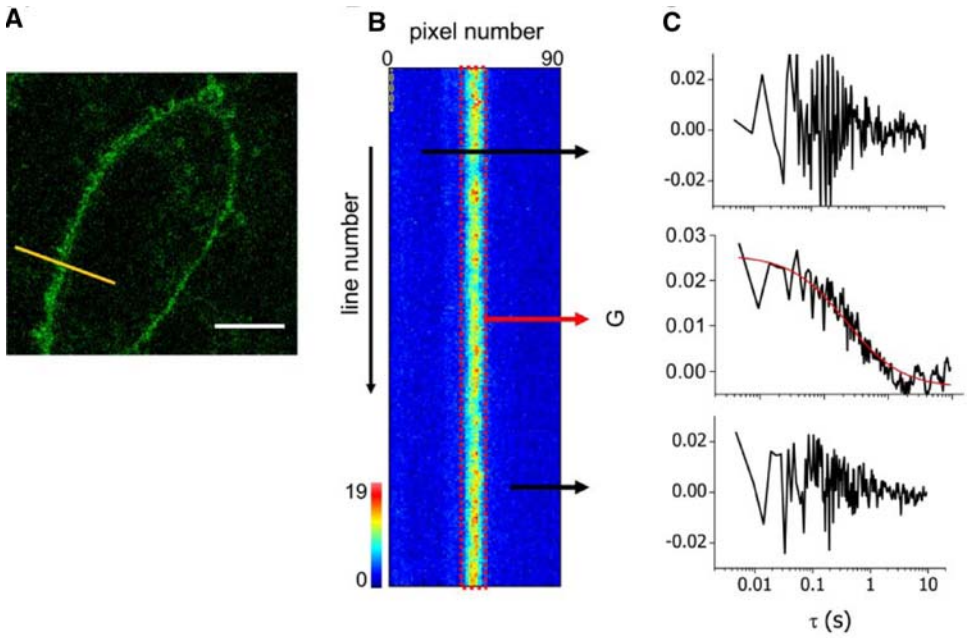

Fig. 7 FCS measurement of AChR diffusion at the plasma membrane of CHO-K1/A5 cells. **a** Image of a cell labeled with alexa^{488}-αBTX. The line traced by the laser is shown in *yellow*. *Bar* 5 μm. **b** Intensity matrix obtained for a representative line-FCS experiment. The intensity is plotted in *pseudocolor*. **c** Temporal autocorrelation functions determined in regions corresponding to the extracellular space (*top*), the plasma membrane (*middle*), and the intracellular compartment (*bottom*). The *continuous line* in the plasma membrane trace corresponds to the fitting of the data with a model considering a value of D of the AChR = 0.04 μm^2 s^{-1}

with the observed decrease in cell-surface AChRs upon CDx treatment (Borroni et al. 2007).

Discussion

Nicotinic acetylcholine receptors are ligand-activated cation channels concentrated in the postsynaptic density which mediate fast excitatory neurotransmission in the peripheral and central nervous system. Concentration of these macromolecules at a synapse is a consequence of the dynamic equilibrium between synthesis, internalization, recycling, and diffusion in/out of the synaptic area. Despite the extensive series of studies undertaken on the AChR, the spatio-temporal distribution of this macromolecule in the membrane and its dependence on environmental lipids remain relatively unexplored.

Table 2 Diffusion coefficients and G_o values of AChR obtained from scanning confocal-FCS

Condition	D (μm^2 s^{-1})	G_o
Control	5.3 ± 0.4 × 10^{-2}	0.028 ± 0.001
10 mM CDx	3.7 ± 0.3 × 10^{-2}**	0.035 ± 0.002*

Single and double asterisks denote statistically significant differences, $P < 0.005$ and $P < 0.001$, respectively

Lipid mobility was explored with a fluorescent analog of each of two lipids characteristically associated with lipid domains: fPEG-Chol and BODIPY-FL-C5-SM. A single-exponential function did not fit well to the FRAP recovery kinetics of fPEG-Chol, suggesting that the mobility of the Chol analog is not a diffusion-limited process. The mobile fraction amounted to roughly 85% (Fig. 1) and Chol depletion did not modify this percentage. Using a phospholipid probe (DPPE) Crane and Verkman (2008) recently found a similar amount of the mobile fraction, also not affected by Chol depletion (Chol removal lowered the diffusion coefficient by a factor of approximately two). D values of ~8.3 and 5.2 × 10^{-2} μm^2 s^{-1} were found for fPEG-Chol and BODIPY-FL-C$_5$-SM, respectively. These values are in the range of the D values (1–1 × 10^{-2}μm^2 s^{-1}) determined by FRAP (Criado et al. 1982b; Johnson et al. 1996; Ladha et al. 1994; Pucadyil et al. 2007; Pucadyil and Chattopadhyay 2006; Schootemeijer et al. 1994; Vaz et al. 1982). The D value for fPEG-Chol decreased ~30% upon Chol depletion. Similarly, Pucadyil and Chattopadhyay (2006) found that DilC$_{18}$, a fluorescent lipid probe sensing ordered lipid domains, is more sensitive to Chol levels than *FAST* DiI, a lipid probe purported to partition favorably in more fluid domains.

As expected, the lateral diffusion of the fluorescent-tagged AChR was found to be slower than that of the lipid probes fPEG-Chol and BODIPY-FL-C$_5$-SM (Figs. 1, 2, 3;

Table 1). Using FRAP, Axelrod et al. (1976) reported two populations of plasma membrane AChRs in primary culture myotubes: an essentially immobile AChR fraction, forming patches of ~20–60 μm and with D values of $<10^{-4}$ μm^2 s^{-1} (Axelrod et al. 1976; Stya and Axelrod 1984) and a mobile fraction consisting of diffusely distributed AChRs (as judged by wide-field fluorescence microscopy) exhibiting distinct, albeit slow, translational mobility (D ~0.5×10^{-2} μm^2 s^{-1}). Here, D of αBTX-labeled AChRs in CHO-K1/A5 cells was estimated to be 0.46×10^{-2} μm^2 s^{-1} (c.f. Table 1), indicating that the lateral diffusion coefficient of the AChR at the cell surface of these cells is very similar to that of the more mobile AChR fraction in developing rat myotubes (0.5×10^{-2} μm^2 s^{-1}; Axelrod et al. 1976) and that of diffusely distributed AChR in adult rat muscle fibers in cell culture (0.25×10^{-2} μm^2 s^{-1}; Stya and Axelrod 1983, 1984).

Nicotinic acetylcholine receptor diffusion was substantially reduced when ~50% plasma membrane Chol was removed by CDx treatment. It should be stressed that Chol depletion produces the accelerated internalization of roughly half of the cell-surface AChRs (Borroni et al. 2007), an effect exactly opposite to that observed with other membrane proteins (Kenworthy et al. 2004), and recycling of AChRs is too slow to contribute to the cell-surface pool within the experimentally observed period (Kumari et al. 2008). Thus, FRAP recovery kinetics upon Chol depletion reflect almost exclusively the behavior of those receptors (~50%) remaining at the cell surface. Most (~80%) of these AChRs were immobile, in contrast with those in control cells (~50%) and the D of the mobile receptors fell by ~40% (Table 1). Loading of CHO-K1/A5 cell with exogenous Chol via CDx–Chol complexes increased the lateral mobility of AChR at the cell surface without affecting Mf (Table 1). Mobility of membrane proteins can vary widely in mammalian cells, from 0 to 85%, and Chol depletion slows down the mobility of both "raft" and "non-raft" proteins (c.f. Kenworthy et al. 2004). The ensemble techniques employed in the current study, FRAP and FCS, fall short of unambiguously detecting motional heterogeneity in the AChRs total pool. The possibility remains therefore that Chol depletion leads to the internalization of only the more mobile AChR pool, leaving behind the less mobile pool reflected in the observed lower AChR mobility after CDx treatment. Single-molecule tracking experiments may prove useful to elucidate this issue.

The influence of Chol content on AChR mobility at the plasma membrane was also studied by confocal FCS. Chol depletion was again found to slow down the diffusion of the receptor: a 30% diminution in the diffusion coefficient of the AChR in CDx-treated cells was observed compared with controls (Table 2), in agreement with FRAP studies. Higher apparent D values were obtained with FCS (Tables 1, 2). Adkins et al. (2007) analyzed the plasma membrane mobility of the dopamine transporter using FRAP and FCS and found similar trends. These authors speculate that the difference stems from the fact that the two techniques sample different environments: FCS would report on fast movements within confined domains whereas FRAP would correspondingly report on long-range diffusion between membrane domains (Adkins et al. 2007; Guo et al. 2008). Additionally, standard FCS techniques do not detect immobile molecules (Bates et al. 2006). Guo et al. (2008) observe that the difference between FCS and FRAP is possibly a result of the very different length scales observed in these two experiments. FCS measures diffusion on a diffraction-limited spot (<500 nm diameter) whereas FRAP measures diffusion on areas a hundred times larger (5–6 μm).

In FRAP experiments performed on cells treated with mevinolin, a statin that inhibits Chol biosynthesis, we found that AChR mobility was affected in a manner similar to that reported here using CDx-mediated acute Chol depletion. Kojro et al. (2001) did not observe changes on plasma membrane fluidity after lovastatin (mevinolin) treatment, at variance with their findings using CDx-mediated Chol depletion. On the basis of these observations, we can conclude that plasma membrane fluidity is not the main factor determining AChR mobility upon Chol depletion.

Several FRAP studies have shown that Chol depletion affects the mobility of various proteins at the plasma membrane although the nature, extent, and sign of the changes remain a contentious subject. Some authors report that the mobility of raft and non-raft resident proteins decreases when Chol is removed from the plasma membrane (Kenworthy et al. 2004; O'Connell and Tamkun 2005; Shvartsman et al. 2003). Restricted diffusion of membrane proteins upon Chol depletion is believed to result from the formation of solid-like clusters in the membrane (Nishimura et al. 2006; Vrljic et al. 2005). Using single-molecule tracking methods, Orr et al. (2005) found that Chol depletion causes confinement of the epidermal growth factor receptor (EGFR) and human epidermal growth factor receptor 2 (HER2) mobility whereas Chol enrichment extended the boundaries of the mobility-restricted areas. In contrast, other authors observed an increase in the lateral mobility of the raft-resident proteins CD44 and wild-type GFP-H-Ras after Chol depletion (Niv et al. 2002; Oliferenko et al. 1999).

Cytoskeletal interactions have been shown to modulate the diffusion and confinement of several membrane proteins (Kusumi et al. 2005; Suzuki et al. 2005; Triller and Choquet 2003). There is also evidence of interactions between lipids, lipid domains, and the cytoskeleton (Lenne

et al. 2006; Maxfield 2002; Niggli 2001). According to Kwik et al. (2003) Chol depletion has general effects on the architecture and function of the membrane, making the sub-membrane cytoskeleton and, in particular, the cortical actin network more stable; actin reorganization would be associated with reduced receptor mobility. Sun et al. (2007) postulate that Chol affects the mechanical properties of plasma membrane through the underlying cytoskeleton. In recent work we determined that Chol depletion affected the long-range relationship of AChR nano-clusters of ~55 nm diameter, changing from a random to a non-random distribution (within a radius of 0.5–1.5 μm) upon Chol depletion (Kellner et al. 2007). Interactions of these nano-clusters with the cytoskeleton were invoked as a possible explanation of these changes, because AChR mobility at the plasma membrane seems to be sensitive to the integrity of the cytoskeleton (Bloch et al. 1989; Dai et al. 2000; Pumplin 1989; Stya and Axelrod 1983). Furthermore, interaction between AChR molecules and the cytoskeleton is of physiological and developmental importance: it is a requisite step in the formation and stability of the neuromuscular junction (Hoch 1999). Although Chol depletion-induced loss of AChR mobility was partially restored in cells incubated with latrunculin A (Table 1), the percentage of mobile AChRs (Mf) in these cells did not reach control levels. From this we can conclude that although the cortical actin meshwork is likely to be involved in receptor mobility at the cell surface in Chol-depleted cells, it need not be the only factor mediating Chol effects on AChR translational diffusion. Other cortical cytoskeletal proteins and/or actin-binding proteins may be involved, and direct interactions of Chol with the AChR may also be implicated. Furthermore, inhibition of actin polymerization by cytochalasin D, which binds to the barbed end of the actin filament and blocks monomer addition, resulting in inhibition of AChR internalization (Kumari et al. 2008). However, direct effects of Chol on the AChR cannot be discarded when considering the effect on the macromolecule's cell surface mobility.

The AChR mobile fraction may correspond to the AChR oligomeric forms observed in negatively stained electron micrographs (Barrantes 1982), which are exchangeable with relatively less mobile AChR aggregates in larger nano-clusters (Kellner et al. 2007). In this hypothesis Chol depletion would affect mostly the more rapidly diffusing AChRs, because of enhanced AChR–AChR interactions, which would reduce their residence time at the cell surface (Barrantes 2007) and result in their internalization (Borroni et al. 2007). Sieber et al. (2007) proposed a model for syntaxin molecule self-organization at the plasma membrane, whereby weak homophilic protein–protein interactions would be responsible for syntaxin clustering. On the basis of transmission electron microscopy experiments of plasma membrane sheets, Lillemeier et al. (2006) proposed a "protein island" model, in which proteins localize to "protein-philic" membrane compartments.

A series of recent publications emphasizes the importance of membrane Chol in the biogenesis and stability of AChR clusters in vivo and in vitro. Chol was found to affect the formation of micron-sized AChR clusters induced by agrin (Campagna and Fallon 2006). Signaling via the agrin/MuSK complex and interaction between the receptor and rapsyn seems to involve lipid platforms (Zhu et al. 2006). Using Laurdan two-photon fluorescence microscopy Stetzkowski-Marden et al. (2006) concluded that AChR clusters reside in ordered membrane domains, a biophysical property characteristic of solid-like lipid domains. Willmann et al. (2006) proposed that Chol-rich lipid microdomains and Src-family kinases both contribute to stabilizing the postsynaptic components. In our experimental system there are no AChR-clustering proteins such as rapsyn and tyrosine kinases, so homophilic protein–protein interaction and links with the actin cytoskeleton are more likely candidates for maintaining the AChR nano-cluster assemblies.

Summarizing, these results show that the neutral lipid Chol modulates cell-surface diffusion of the muscle-type AChR in a mammalian cell. Chol could thus have an important homeostatic function in the maintenance of receptor levels and dynamics at the cholinergic synapse.

Acknowledgments Thanks are due to Professor Toshihide Kobayashi and Dr Satoshi B. Sato, of the Lipid Biology Laboratory, RIKEN Institute of Physical and Chemical Research, Discovery Research Institute, Saitama, and Department of Biophysics, Kyoto University, Japan, for providing a sample of f-PEG-Chol, and to Dr Jorge J. Wenz and Ms Virginia Borroni for helpful discussion. Research described in this article was supported in part by PICT 01-12790 and 5-20155 from FONCYT, Ministry of Science and Technology; PIP No. 6367 from the Argentinian Scientific Research Council (CONICET); Philip Morris USA Inc., and Philip Morris International; and PGI No. 24/B135 from Universidad Nacional del Sur, Argentina, to F.J.B.

References

Adkins EM, Samuvel DJ, Fog JU, Eriksen J, Jayanthi LD, Vaegter CB, Ramamoorthy S, Gether U (2007) Membrane mobility and microdomain association of the dopamine transporter studied with fluorescence correlation spectroscopy and fluorescence recovery after photobleaching. Biochemistry 46:10484–10497

Axelrod D (1980) Crosslinkage and visualization of acetylcholine receptors on myotubes with biotinylated alpha-bungarotoxin and fluorescent avidin. Proc Natl Acad Sci USA 77:4823–4827

Axelrod D, Ravdin P, Koppel DE, Schlessinger J, Webb WW, Elson EL, Podleski TR (1976) Lateral motion of fluorescently labeled acetylcholine receptors in membranes of developing muscle fibers. Proc Natl Acad Sci USA 73:4594–4598

Barrantes FJ (1979) Endogenous chemical receptors: some physical aspects. Annu Rev Biophys Bioeng 8:287–321

Barrantes FJ (1982) Oligomeric forms of the membrane-bound acetylcholine receptor disclosed upon extraction of the Mr 43,000 nonreceptor peptide. J Cell Biol 92:60–68

Barrantes FJ (1989) The lipid environment of the nicotinic acetylcholine receptor in native and reconstituted membranes. Crit Rev Biochem Mol Biol 24:437–478

Barrantes FJ (1993) Structural–functional correlates of the nicotinic acetylcholine receptor and its lipid microenvironment. FASEB J 7:1460–1467

Barrantes FJ (2003) Modulation of nicotinic acetylcholine receptor function through the outer and middle rings of transmembrane domains. Curr Opin Drug Discov Dev 6:620–632

Barrantes FJ (2004) Structural basis for lipid modulation of nicotinic acetylcholine receptor function. Brain Res Brain Res Rev 47:71–95

Barrantes FJ (2007) Cholesterol effects on nicotinic acetylcholine receptor. J Neurochem 103(Suppl 1):72–80

Bates IR, Wiseman PW, Hanrahan JW (2006) Investigating membrane protein dynamics in living cells. Biochem Cell Biol 84:825–831

Bloch RJ, Velez M, Krikorian JG, Axelrod D (1989) Microfilaments and actin-associated proteins at sites of membrane-substrate attachment within acetylcholine receptor clusters. Exp Cell Res 182:583–596

Borroni V, Baier CJ, Lang T, Bonini I, White MM, Garbus I, Barrantes FJ (2007) Cholesterol depletion activates rapid internalization of submicron-sized acetylcholine receptor domains at the cell membrane. Mol Membr Biol 24:1–15

Bruses JL, Chauvet N, Rutishauser U (2001) Membrane lipid rafts are necessary for the maintenance of the (alpha)7 nicotinic acetylcholine receptor in somatic spines of ciliary neurons. J Neurosci 21:504–512

Campagna JA, Fallon J (2006) Lipid rafts are involved in C95 (4, 8) agrin fragment-induced acetylcholine receptor clustering. Neuroscience 138:123–132

Chen Y, Lagerholm BC, Yang B, Jacobson K (2006) Methods to measure the lateral diffusion of membrane lipids and proteins. Methods 39:147–153

Christian AE, Haynes MP, Phillips MC, Rothblat GH (1997) Use of cyclodextrins for manipulating cellular cholesterol content. J Lipid Res 38:2264–2272

Corbin J, Wang HH, Blanton MP (1998) Identifying the cholesterol binding domain in the nicotinic acetylcholine receptor with [125I]azido-cholesterol. Biochim Biophys Acta 1414:65–74

Coue M, Brenner SL, Spector I, Korn ED (1987) Inhibition of actin polymerization by Latrunculin A. FEBS Lett 213:316–318

Crane JM, Verkman AS (2008) Long-range nonanomalous diffusion of quantum dot-labeled aquaporin-1 water channels in the cell plasma membrane. Biophys J 94:702–713

Criado M, Eibl H, Barrantes FJ (1982a) Effects of lipids on acetylcholine receptor. Essential need of cholesterol for maintenance of agonist-induced state transitions in lipid vesicles. Biochemistry 21:3622–3629

Criado M, Vaz WL, Barrantes FJ, Jovin TM (1982b) Translational diffusion of acetylcholine receptor (monomeric and dimeric forms) of Torpedo marmorata reconstituted into phospholipid bilayers studied by fluorescence recovery after photobleaching. Biochemistry 21:5750–5755

Dai Z, Luo X, Xie H, Peng HB (2000) The actin-driven movement and formation of acetylcholine receptor clusters. J Cell Biol 150:1321–1334

Edidin M (1994) Fluorescence photobleaching and recovery, FPR, in the analysis of membrane structure and dynamics. In: Damjanovich S, Edidin M, Szollosi J, Tron L (eds) Mobility and proximity in biological membranes. CRC Press, Boca Raton, pp 109–135

Edidin M (2003) Lipids on the frontier: a century of cell-membrane bilayers. Nat Rev Mol Cell Biol 4:414–418

Ellenberg J, Siggia ED, Moreira JE, Smith CL, Presley JF, Worman HJ, Lippincott-Schwartz J (1997) Nuclear membrane dynamics and reassembly in living cells: targeting of an inner nuclear membrane protein in interphase and mitosis. J Cell Biol 138:1193–1206

Guo L, Har JY, Sankaran J, Hong Y, Kannan B, Wohland T (2008) Molecular diffusion measurement in lipid bilayers over wide concentration ranges: a comparative study. Chemphyschem 9:721–728

Hao M, Mukherjee S, Maxfield FR (2001) Cholesterol depletion induces large scale domain segregation in living cell membranes. Proc Natl Acad Sci USA 98:13072–13077

Hoch W (1999) Formation of the neuromuscular junction. Agrin and its unusual receptors. Eur J Biochem 265:1–10

Ishitsuka R, Sato SB, Kobayashi T (2005) Imaging lipid rafts. J Biochem 137:249–254

Jacobson K, Mouritsen OG, Anderson RG (2007) Lipid rafts: at a crossroad between cell biology and physics. Nat Cell Biol 9:7–14

Johnson ME, Berk DA, Blankschtein D, Golan DE, Jain RK, Langer RS (1996) Lateral diffusion of small compounds in human stratum corneum and model lipid bilayer systems. Biophys J 71:2656–2668

Kellner RR, Baier CJ, Willig KI, Hell SW, Barrantes FJ (2007) Nanoscale organization of nicotinic acetylcholine receptors revealed by stimulated emission depletion microscopy. Neuroscience 144:135–143

Kenworthy AK, Nichols BJ, Remmert CL, Hendrix GM, Kumar M, Zimmerberg J, Lippincott-Schwartz J (2004) Dynamics of putative raft-associated proteins at the cell surface. J Cell Biol 165:735–746

Kojro E, Gimpl G, Lammich S, Marz W, Fahrenholz F (2001) Low cholesterol stimulates the nonamyloidogenic pathway by its effect on the alpha-secretase ADAM 10. Proc Natl Acad Sci USA 98:5815–5820

Kumari S, Borroni V, Chaudhry A, Chanda B, Massol R, Mayor S, Barrantes FJ (2008) Nicotinic acetylcholine receptor is internalized via a Rac-dependent, dynamin-independent endocytic pathway. J Cell Biol 181:1179–1193

Kummer TT, Misgeld T, Sanes JR (2006) Assembly of the postsynaptic membrane at the neuromuscular junction: paradigm lost. Curr Opin Neurobiol 16:74–82

Kusumi A, Nakada C, Ritchie K, Murase K, Suzuki K, Murakoshi H, Kasai RS, Kondo J, Fujiwara T (2005) Paradigm shift of the plasma membrane concept from the two-dimensional continuum fluid to the partitioned fluid: high-speed single-molecule tracking of membrane molecules. Annu Rev Biophys Biomol Struct 34:351–378

Kwik J, Boyle S, Fooksman D, Margolis L, Sheetz MP, Edidin M (2003) Membrane cholesterol, lateral mobility, and the phosphatidylinositol 4,5-bisphosphate-dependent organization of cell actin. Proc Natl Acad Sci USA 100:13964–13969

Ladha S, Mackie AR, Clark DC (1994) Cheek cell membrane fluidity measured by fluorescence recovery after photobleaching and steady-state fluorescence anisotropy. J Membr Biol 142:223–228

Leibel WS, Firestone LL, Legler DC, Braswell LM, Miller KW (1987) Two pools of cholesterol in acetylcholine receptor-rich membranes from Torpedo. Biochim Biophys Acta 897:249–260

Lenne PF, Wawrezinieck L, Conchonaud F, Wurtz O, Boned A, Guo XJ, Rigneault H, He HT, Marguet D (2006) Dynamic molecular confinement in the plasma membrane by microdomains and the cytoskeleton meshwork. EMBO J 25:3245–3256

Lillemeier BF, Pfeiffer JR, Surviladze Z, Wilson BS, Davis MM (2006) Plasma membrane-associated proteins are clustered into

islands attached to the cytoskeleton. Proc Natl Acad Sci USA 103:18992–18997
Marchand S, Devillers-Thiery A, Pons S, Changeux JP, Cartaud J (2002) Rapsyn escorts the nicotinic acetylcholine receptor along the exocytic pathway via association with lipid rafts. J Neurosci 22:8891–8901
Marsh D, Barrantes FJ (1978) Immobilized lipid in acetylcholine receptor-rich membranes from Torpedo marmorata. Proc Natl Acad Sci USA 75:4329–4333
Maxfield FR (2002) Plasma membrane microdomains. Curr Opin Cell Biol 14:483–487
Muller JD, Chen Y, Gratton E (2003) Fluorescence correlation spectroscopy. Methods Enzymol 361:69–92
Narayanaswami V, McNamee MG (1993) Protein–lipid interactions and Torpedo californica nicotinic acetylcholine receptor function. 2. Membrane fluidity and ligand-mediated alteration in the accessibility of gamma subunit cysteine residues to cholesterol. Biochemistry 32:12420–12427
Nehls S, Snapp EL, Cole NB, Zaal KJ, Kenworthy AK, Roberts TH, Ellenberg J, Presley JF, Siggia E, Lippincott-Schwartz J (2000) Dynamics and retention of misfolded proteins in native ER membranes. Nat Cell Biol 2:288–295
Niggli V (2001) Structural properties of lipid-binding sites in cytoskeletal proteins. Trends Biochem Sci 26:604–611
Nishimura SY, Vrljic M, Klein LO, McConnell HM, Moerner WE (2006) Cholesterol depletion induces solid-like regions in the plasma membrane. Biophys J 90:927–938
Niv H, Gutman O, Kloog Y, Henis YI (2002) Activated K-Ras and H-Ras display different interactions with saturable nonraft sites at the surface of live cells. J Cell Biol 157:865–872
O'Connell KM, Tamkun MM (2005) Targeting of voltage-gated potassium channel isoforms to distinct cell surface microdomains. J Cell Sci 118:2155–2166
Oliferenko S, Paiha K, Harder T, Gerke V, Schwarzler C, Schwarz H, Beug H, Gunthert U, Huber LA (1999) Analysis of CD44-containing lipid rafts: recruitment of annexin II and stabilization by the actin cytoskeleton. J Cell Biol 146:843–854
Orr G, Hu D, Ozcelik S, Opresko LK, Wiley HS, Colson SD (2005) Cholesterol dictates the freedom of EGF receptors and HER2 in the plane of the membrane. Biophys J 89:1362–1373
Pediconi MF, Gallegos CE, Los Santos EB, Barrantes FJ (2004) Metabolic cholesterol depletion hinders cell-surface trafficking of the nicotinic acetylcholine receptor. Neuroscience 128:239–249
Pucadyil TJ, Chattopadhyay A (2006) Effect of cholesterol on lateral diffusion of fluorescent lipid probes in native hippocampal membranes. Chem Phys Lipids 143:11–21
Pucadyil TJ, Mukherjee S, Chattopadhyay A (2007) Organization and dynamics of NBD-labeled lipids in membranes analyzed by fluorescence recovery after photobleaching. J Phys Chem B 111:1975–1983
Pumplin DW (1989) Acetylcholine receptor clusters of rat myotubes have at least three domains with distinctive cytoskeletal and membranous components. J Cell Biol 109:739–753
Rao M, Mayor S (2005) Use of Forster's resonance energy transfer microscopy to study lipid rafts. Biochim Biophys Acta 1746:221–233
Roccamo AM, Pediconi MF, Aztiria E, Zanello L, Wolstenholme A, Barrantes FJ (1999) Cells defective in sphingolipids biosynthesis express low amounts of muscle nicotinic acetylcholine receptor. Eur J Neurosci 11:1615–1623
Ruan Q, Cheng MA, Levi M, Gratton E, Mantulin WW (2004) Spatial–temporal studies of membrane dynamics: scanning fluorescence correlation spectroscopy (SFCS). Biophys J 87:1260–1267
Sato SB, Ishii K, Makino A, Iwabuchi K, Yamaji-Hasegawa A, Senoh Y, Nagaoka I, Sakuraba H, Kobayashi T (2004) Distribution and transport of cholesterol-rich membrane domains monitored by a membrane-impermeant fluorescent polyethylene glycol-derivatized cholesterol. J Biol Chem 279:23790–23796
Schootemeijer A, Van Beekhuizen AE, Gorter G, Tertoolen LG, De Laat SW, Akkerman JW (1994) Rapid alterations in lateral mobility of lipids in the plasma membrane of activated human megakaryocytes. Eur J Biochem 221:353–362
Shvartsman DE, Kotler M, Tall RD, Roth MG, Henis YI (2003) Differently anchored influenza hemagglutinin mutants display distinct interaction dynamics with mutual rafts. J Cell Biol 163:879–888
Sieber JJ, Willig KI, Kutzner C, Gerding-Reimers C, Harke B, Donnert G, Rammner B, Eggeling C, Hell SW, Grubmuller H, Lang T (2007) Anatomy and dynamics of a supramolecular membrane protein cluster. Science 317:1072–1076
Simons K, Ikonen E (1997) Functional rafts in cell membranes. Nature 387:569–572
Simons K, van Meer G (1988) Lipid sorting in epithelial cells. Biochemistry 27:6197–6202
Spector I, Shochet NR, Blasberger D, Kashman Y (1989) Latrunculins—novel marine macrolides that disrupt microfilament organization and affect cell growth: I. Comparison with cytochalasin D. Cell Motil Cytoskeleton 13:127–144
Stetzkowski-Marden F, Gaus K, Recouvreur M, Cartaud A, Cartaud J (2006) Agrin elicits membrane lipid condensation at sites of acetylcholine receptor clusters in C2C12 myotubes. J Lipid Res 47:2121–2133
Stya M, Axelrod D (1983) Mobility and detergent extractability of acetylcholine receptors on cultured rat myotubes: a correlation. J Cell Biol 97:48–51
Stya M, Axelrod D (1984) Mobility of extrajunctional acetylcholine receptors on denervated adult muscle fibers. J Neurosci 4:70–74
Sun M, Northup N, Marga F, Huber T, Byfield FJ, Levitan I, Forgacs G (2007) The effect of cellular cholesterol on membrane-cytoskeleton adhesion. J Cell Sci 120:2223–2231
Suzuki K, Ritchie K, Kajikawa E, Fujiwara T, Kusumi A (2005) Rapid hop diffusion of a G-protein-coupled receptor in the plasma membrane as revealed by single-molecule techniques. Biophys J 88:3659–3680
Triller A, Choquet D (2003) Synaptic structure and diffusion dynamics of synaptic receptors. Biol Cell 95:465–476
Vaz WL, Criado M, Madeira VM, Schoellmann G, Jovin TM (1982) Size dependence of the translational diffusion of large integral membrane proteins in liquid-crystalline phase lipid bilayers. A study using fluorescence recovery after photobleaching. Biochemistry 21:5608–5612
Vrljic M, Nishimura SY, Moerner WE, McConnell HM (2005) Cholesterol depletion suppresses the translational diffusion of class II major histocompatibility complex proteins in the plasma membrane. Biophys J 88:334–347
Willmann R, Pun S, Stallmach L, Sadasivam G, Santos AF, Caroni P, Fuhrer C (2006) Cholesterol and lipid microdomains stabilize the postsynapse at the neuromuscular junction. EMBO J 25:4050–4060
Zaal KJ, Smith CL, Polishchuk RS, Altan N, Cole NB, Ellenberg J, Hirschberg K, Presley JF, Roberts TH, Siggia E, Phair RD, Lippincott-Schwartz J (1999) Golgi membranes are absorbed into and reemerge from the ER during mitosis. Cell 99:589–601
Zhu D, Xiong WC, Mei L (2006) Lipid rafts serve as a signaling platform for nicotinic acetylcholine receptor clustering. J Neurosci 26:4841–4851